

# New results on the direct observations of thermal radio emission from a solar coronal mass ejection

R. Ramesh<sup>1</sup>, A. Kumari<sup>1,3</sup>, C. Kathiravan<sup>1</sup>, D. Ketaki<sup>1,2</sup>, T. J. Wang<sup>4,5</sup>

<sup>1</sup>Indian Institute of Astrophysics, Koramangala 2nd Block, Bangalore, Karnataka, India - 560034

<sup>2</sup>Department of Physics, Sir Parashurambhau College, Pune, Maharashtra, India - 411 030

<sup>3</sup>Department of Physics, University of Helsinki, P.O. Box 64, FI-00014 Helsinki, Finland

<sup>4</sup>Department of Physics, The Catholic University of America, Washington, DC 20064, USA

<sup>5</sup>NASA Goddard Space Flight Center, Code 671, Greenbelt, MD 20771, USA

## Key Points:

- We report observations of thermal radio emission from the frontal structure of a CME simultaneously at 80 MHz and 53 MHz.
- The electron density, mass and magnetic field of the CME were estimated directly from the observed thermal radio emission.
- Similar observations with larger low frequency radio antenna arrays like LOFAR and SKA are expected to be useful to understand CMEs.

arXiv:2103.04148v1 [astro-ph.SR] 6 Mar 2021

---

Corresponding author: R. Ramesh, [ramesh@iiap.res.in](mailto:ramesh@iiap.res.in)

## Abstract

We report observations of thermal emission from the frontal structure of a coronal mass ejection (CME) using data obtained with the Gauribidanur RAdioheliograPH (GRAPH) simultaneously at 80 MHz and 53 MHz on 2016 May 1. The CME was due to activity on the far-side of the Sun, but near its limb. No non-thermal radio burst activity were noticed. This provided an opportunity to observe the faint thermal radio emission from the CME, and hence directly estimate the electron density, mass, and magnetic field strength of the plasma entrained in the CME. Considering that CMEs are mostly observed only in whitelight and reports on their plasma characteristics are also limited, the rare direct radio observations of thermal emission from a CME and independent diagnosis of its plasma parameters are important measurements in the field of CME physics.

## 1 Introduction

CMEs are large scale and energetic eruptions in the solar atmosphere during which  $\approx 10^{12}$ - $10^{16}$ g of magnetized coronal plasma are ejected into the heliosphere at speeds ranging from  $\approx 100$ - $3000$ km/s (e.g., Vourlidas et al., 2010). They are mostly observed in whitelight using coronagraphs which use an occulter to block the bright light from the solar photosphere so that structures like CMEs can be observed with better contrast. But the size of the coronagraph occulters till date has always been larger than that of the photosphere. For example, in the *Large Angle and Spectrometric Coronagraph C2* (LASCO C2; Brueckner et al., 1995) on board the *Solar and Heliospheric Observatory* (SOHO), the occulter covers a heliocentric distance ( $r$ ) of  $\approx 2.2R_{\odot}$ , where  $R_{\odot}$  is the radius of the photosphere. This prevents observations of the corona present immediately off the solar limb, in addition to the corona above the solar disk. Radio observations are unique in this connection since there is no occulter. The radio emission associated with and/or from the CMEs can be divided into two classes, thermal and non-thermal (e.g., Vourlidas, 2004). In the non-thermal case, type IV radio bursts due to gyrosynchrotron and/or plasma emission from the electrons in the CME (Stewart et al., 1974; Wagner et al., 1981; Gary et al., 1985; Gopalswamy & Kundu, 1987, 1989, 1990; Bastian et al., 2001; Maia et al., 2007; Ramesh et al., 2013; Tun & Vourlidas, 2013; Bain et al., 2014; Sasikumar Raja et al., 2014; Hariharan et al., 2016a; Carley et al., 2017; Morosan et al., 2019; Vasanth et al., 2019; Mondal et al., 2020), type II radio bursts due to plasma emission from the electrons accelerated by MHD shocks driven by the CME (Stewart et al., 1974; Mann et al., 1995; Aurass, 1997; Gopalswamy, 2006; Ramesh et al., 2010b, 2012a; Kumari et al., 2017a, 2017b; Chrysaphi et al., 2018; Kumari et al., 2019; Maguire et al., 2020), and type I noise storm continuum due to plasma emission from changes in the coronal magnetic field during a CME (Kerdran et al., 1983; Ramesh & Sundaram, 2000a; Kathiravan et al., 2007) have been widely reported. Compared to this, there are only a few reports of direct detection of CMEs at radio frequencies via thermal bremsstrahlung emission (Sheridan et al., 1978; Gopalswamy & Kundu, 1992, 1993; Kathiravan et al., 2002; Kathiravan & Ramesh, 2004, 2005; Ramesh et al., 2003; Ramesh, 2005a). Here we present radio observations of thermal emission from a CME simultaneously at two different frequencies, and compare the nature of the observed emission with published reports. We were fortunate that there were no flare activity on the visible hemisphere of the Sun whose associated non-thermal radio burst activity would have otherwise probably prevented us from observing the comparatively weak thermal radio emission from the CME (e.g., Bastian & Gary, 1997). For example, the peak flux density of the radio burst observed on 2006 December 6 was  $\approx 10^6$ sfu (sfu=solar flux unit= $10^{-22}$ W/m<sup>2</sup>/Hz) in the 1-2 GHz frequency range (Gary, 2019). Compared to this the flux density of thermal radio emission from the ‘quiet’ Sun is  $\sim$ few sfu or even less. This calls for a very large dynamic range to observe the radio burst and the ‘quiet’ Sun simultaneously.

## 2 Observations

The radio observations were carried out on 2016 May 1 using the different facilities in Gauribidanur observatory (<https://www.iiap.res.in/?q=centers/radio>; Ramesh, 2011a, 2014). Two-dimensional images obtained with the *Gauribidanur RAdioheliograPH* (GRAPH; Ramesh et al., 1998, 1999b, 2006b) at 80 MHz and 53 MHz were used to obtain positional information. The observations were carried out close to the local meridian transit time of the Sun ( $\approx 06:30$  UT). For radio spectral data, we used observations with the *Gauribidanur LOw-frequency Solar Spectrograph* (GLOSS; Ebenezer et al., 2001, 2007; Kishore et al., 2014; Hariharan et al., 2016b), *Gauribidanur RAdio Spectro-Polarimeter* (GRASP; Sasikumar Raja et al., 2013; Kishore et al., 2015; Hariharan et al., 2015), and e-CALLISTO (Monstein et al., 2007; Benz et al., 2009). We also used data obtained with the Gauribidanur Radio Interferometric Polarimeter (GRIP; Ramesh & Sastry, 2005b; Ramesh et al., 2008). The combined use of the aforementioned observations help to understand the radio signatures associated with the corresponding solar activity in a better manner (e.g., Sasikumar Raja & Ramesh, 2013). Observations in EUV at 211Å with the *Atmospheric Imaging Assembly* (AIA; Lemen et al., 2012) on board the *Solar Dynamics Observatory* (SDO), and in whitelight with the COR1 coronagraph of the *Sun-Earth Connection Coronal and Heliospheric Investigation* (SECCHI; Howard et al., 2008) on board the *Solar TERrestrial RELationship Observatory* (STEREO) and SOHO/LASCO were used to supplement the radio observations.

Figure 1 shows a composite of the difference images obtained in EUV, whitelight, and radio on 2016 May 1 during the interval  $\approx 6-7$  UT. An inspection of the SOHO/LASCO CME catalog ([https://cdaw.gsfc.nasa.gov/CME\\_list/UNIVERSAL/2016.05/univ2016\\_05.html](https://cdaw.gsfc.nasa.gov/CME_list/UNIVERSAL/2016.05/univ2016_05.html)) indicates that close to the above epoch a CME was observed around position angle (PA, measured counter clockwise from the solar north)  $\approx 50^\circ$ . The enhanced whitelight emission in Figure 1 corresponds to the frontal structure of the aforementioned CME. It was a narrow CME without the three-part structure associated with a typical CME. No streamer-blowout was also noticed ([https://lasco-www.nrl.navy.mil/carr\\_maps/c2/](https://lasco-www.nrl.navy.mil/carr_maps/c2/)). Its various characteristics estimated from the SOHO-LASCO observations are, angular width  $\approx 36^\circ$ ; linear speed in the plane-of-sky  $\approx 482$  km/s; acceleration  $\approx -10$  m/s<sup>2</sup>; mass  $\approx 1.2 \times 10^{15}$  g; kinetic energy  $\approx 1.4 \times 10^{30}$  erg. An inspection of the SDO/AIA-211Å data indicates that the CME was most likely due to activity in the sunspot region AR12541 located at  $\approx N01E94$  ([https://www.lmsal.com/solarsoft/ssw/last\\_events-2016/last\\_events\\_20160503\\_1121/index.html](https://www.lmsal.com/solarsoft/ssw/last_events-2016/last_events_20160503_1121/index.html)). Since the region was just behind the limb, any projection effects on the aforementioned CME parameters will be very minimal. We verified the activity in AR12541 using STEREO-A/EUVI 195Å difference images. STEREO-A was at  $\approx E160^\circ$  during the above period ([https://stereo-ssc.nascom.nasa.gov/cgi-bin/make\\_where\\_gif](https://stereo-ssc.nascom.nasa.gov/cgi-bin/make_where_gif)). This implies that AR12541 was located at  $\approx 24^\circ$  inside the limb for STEREO-A view (see Panels a-c in Figure 2).

The GRAPH observations in Figure 1 were close to  $\approx 06:47$  UT at 53 MHz and 80 MHz simultaneously. The spatio-temporal correspondence between the radio contours and the whitelight CME indicates that the radio emission could be due to the CME. The larger size of the radio contours, particularly at 53 MHz and in the north-south direction, are likely due to the comparatively limited angular resolution of GRAPH ( $\approx 4' \times 6'$  (R.A.  $\times$  decl.) and  $\approx 6' \times 9'$  at 80 MHz and 53 MHz, respectively.) The EUV eruptive activity noticed near the solar limb indicate the source region and the early phase of the CME. Though it appears that the EUV eruption is slightly displaced from the whitelight and radio structures, an inspection of the 12 sec running difference images using SDO/AIA-211Å and SDO/AIA-193Å indicate that the eruptive activity rises up non-radially in the direction towards the locations of the whitelight and radio structures at a later time.

The centroids of the radio emission in Figure 1 are located at  $r_{80} \approx 1.7 \pm 0.2 R_\odot$  (80 MHz) and  $r_{53} \approx 2.1 \pm 0.2 R_\odot$  (53 MHz). Any possible error in the position of the centroids due to propagation effects such as scattering by density inhomogeneities in the solar corona

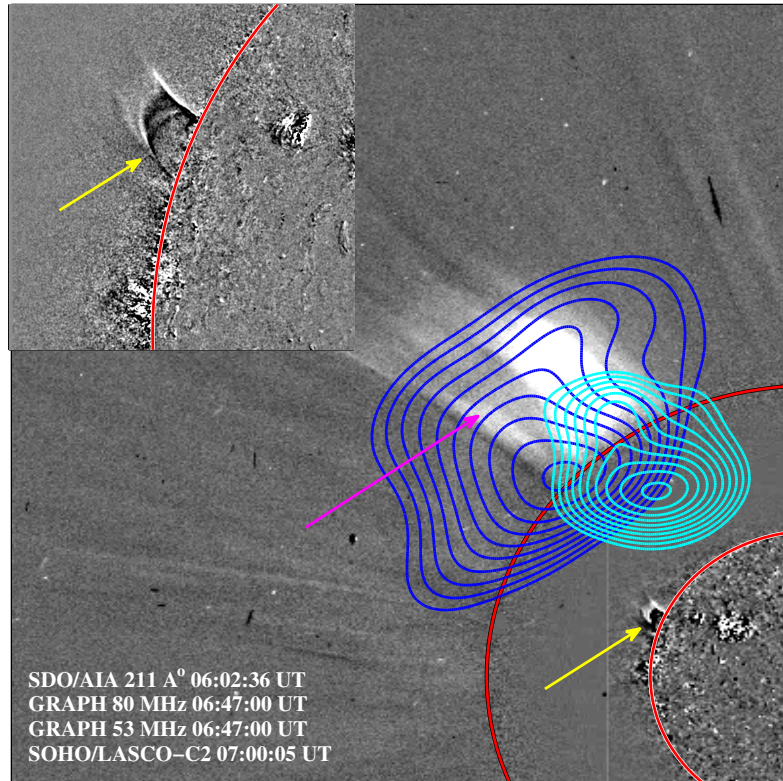


**Figure 1.** A composite of the difference images obtained using EUV ( $\approx 06:02-05:41$  UT), radio ( $\approx 06:47-06:42$  UT), and whitelight ( $\approx 07:00-06:00$  UT) observations on 2016 May 1. The inner and outer ‘red’ circles indicate the solar limb (radius  $\approx 1R_{\odot}$ ), and the occulter in the SOHO/LASCO-C2 coronagraph (radius  $\approx 2.2R_{\odot}$ ). The bright emission above the occulter (indicated by ‘magenta’ arrow) is the whitelight CME. The inset in the upper left corner is a close-up view of the region indicated by the ‘yellow’ arrow on the SDO/AIA-211Å image. The ‘cyan’ and ‘blue’ contours correspond to radio observations at 80 MHz and 53 MHz. The contour levels are  $\approx [63, 67, 71, 75, 79, 83, 87, 91, 95, 99]\%$  of  $3.4 \times 10^5$  K (80 MHz) and  $0.8 \times 10^5$  K (53 MHz).

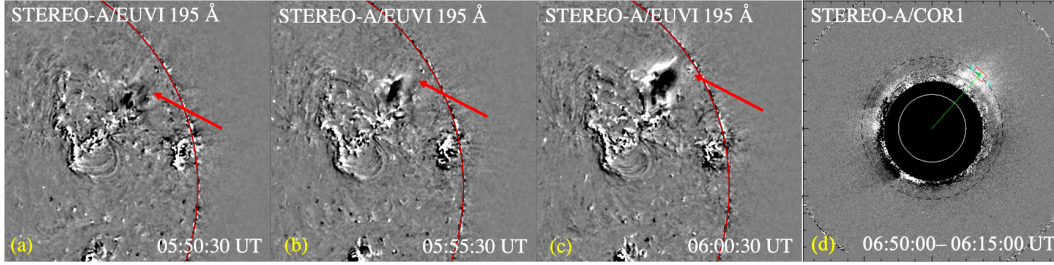


**Figure 2.** Panels (a)-(c) are the STEREO-A/EUVI 195Å running difference images of activity in AR12541 (indicated by ‘red’ arrow) on 2016 May 1. The ‘red’ circle indicate the solar limb. Panel (d) is the STEREO-A/COR1 pB difference image obtained on the same day. The ‘white’ and ‘black’ circles indicate the solar limb and the coronagraph occulter (radius  $\approx 1.4R_{\odot}$ ), respectively. The enhanced emission to the upper right of the occulter corresponds to the same CME in Figure 1. Its electron density ( $N_e^{cor1a}$ ) was estimated from the region covered by the ‘red’ box.

and/or refraction in the Earth’s ionosphere is expected to be within the above error limit (Stewart & McLean, 1982; Ramesh et al., 1999a, 2012b; Kathiravan et al., 2011; Mugundhan et al., 2016, 2018a). The fact that the Sun is presently going through a period of extended minimum (during which the observations reported in the present work were carried out) indicates that the effects of scattering are likely to be less pronounced (Sasikumar Raja et al., 2016; Mugundhan et al., 2017; Ramesh et al., 2020). Furthermore, the observations were carried out close to the local noon during which time the zenith angle of the Sun is the least. Possible positional shifts in hour angle and declination due to ionospheric effects are expected to be negligible during that time. Note that the elevation of Sun on 2016 May 1 when the present observations were carried out was  $\approx 88^{\circ}$ . Secondly, the 53 MHz and 80 MHz radio images in Figure 1 were obtained by subtracting the corresponding radio images obtained  $\approx 5$ min earlier at the respective frequencies. This time interval is lesser than the period ( $\approx 20$ min) over which radio source positions at low frequencies usually change due to ionospheric effects (Stewart & McLean, 1982; Mercier, 1996). The brightness temperatures ( $T_b$ ) of the radio sources in Figure 1 near their centroids are  $T_b^{80} \approx 3.4 \times 10^5$  K (80 MHz) and  $T_b^{53} \approx 0.8 \times 10^5$  K (53 MHz). The corresponding flux density ( $S$ ) values are  $S_{80} \approx 0.14$ sfu (80 MHz) and  $S_{53} \approx 0.06$ sfu (53 MHz). The spectral index ( $\alpha$ ) derived from the above flux densities is  $\approx 2.1$ . These are in agreement with that reported for thermal emission from the solar corona at low frequencies (Erickson et al., 1977; Sheridan & McLean, 1985; K. R. Subramanian & Sastry, 1988; Ramesh et al., 2000b, 2006a, 2010a). Furthermore, no non-thermal radio bursts were observed either elsewhere (<ftp://ftp.swpc.noaa.gov/pub/warehouse>) or with GLOSS or GRASP during the particular observing period. Therefore it is likely that the enhanced radio emission in Figure 1 is thermal in nature. The contrast of such emission is generally better at frequencies  $< 100$  MHz (e.g., Lantos et al., 1987). Model calculations by Bastian and Gary (1997) also indicate that it is possible to observe enhanced thermal emission from particularly the off-limb CMEs using difference images as in the present case. The above  $T_b$  values are reasonably consistent with those predicted by the aforementioned model for thermal emission from a ‘typical’ CME in the same frequency range. Note that for non-thermal gyrosynchrotron emission from a CME, the  $T_b$  values predicted by the model are higher than the aforementioned observed  $T_b$  values by about factor of four, even for the lowest values assumed for the different parameters in the model. Low frequency observations reported earlier also indicate that the observed  $T_b$  of gyro-synchrotron emission from a CME are  $\sim 10^7 - 10^8$  K (Wagner et al., 1981; Gary et al., 1985; Dulk, 1985; Gopalswamy & Kundu, 1987, 1990; Sasikumar Raja et al., 2014).

Figure 3 shows the GRIP observations in the transit mode at 80 MHz on 2016 April 30, May 1, and May 2 around  $\approx 06:48$  UT. The half-power width of the response pattern of GRIP at the above frequency is  $\approx 1.8^\circ$ . Since this is wider than the size of the Sun, the observations in Figure 3 correspond to integrated emission from the ‘whole’ Sun at 80 MHz. The gradual increase/decrease in the observed correlation count is due to the passage of Sun across the response pattern of GRIP. There is noticeable Stokes V emission on 2016 May 1 with a peak correlation count of  $\approx 15$ . No similar emission was observed on 2016 April 30 and May 2. The Stokes I emission on 2016 May 1 also shows an increase of  $\approx 125$  counts as compared to the observations on 2016 May 2 (i.e. from  $\approx 225$  to  $\approx 350$  counts). The Sun was ‘quiet’ on 2016 April 30 too, but the peak Stokes I correlation count ( $\approx 255$ ) was slightly higher. Following Kundu et al. (1977), we used 2016 May 2 observations as the reference value for ‘quiet’ Sun to estimate the aforementioned increase in the Stokes I correlation count on 2016 May 1. Based on the above, we calculated the degree of circular polarization ( $dcp = \frac{|V|}{I}$ ) for the observations on 2016 May 1, and the value is  $\approx 12\%$ . This is lesser than the  $dcp$  reported for non-thermal gyrosynchrotron radio emission from CME associated radio emission in the similar frequency range (Dulk, 1985; Sasikumar Raja et al., 2014). The absence of radio bursts during our observing period on 2016 May 1 argue against any non-thermal origin for the observed Stokes V emission (e.g., Mugundhan et al., 2018b). The possibility of non-thermal noise storm continuum emission too can be ruled out since the sunspot region AR12541 in which there was activity that day was behind the limb as mentioned earlier and noise storm sources are highly directive (Ramesh et al., 2011b). Coincidentally, the GRIP observations on 2016 May 1 was nearly at the same time as the GRAPH observations in Figure 1. One of the observing frequencies with the GRAPH (80 MHz) was also same as that of the GRIP. Therefore it is possible that the observed Stokes V emission on 2016 May 1 in Figure 3 could be due to the enhanced thermal emission above the limb in Figure 1 at the same frequency (Sastry, 2009; Ramesh et al., 2010a). Note that the thermal emission could be circularly polarized in the presence of a magnetic field. Since the medium becomes birefringent due to the latter, the randomly polarized thermal radiation propagates in two orthogonal circular modes, i.e., the ordinary (‘o’) and the extraordinary (‘e’) mode. A difference between the optical depths and hence the  $T_b$  of the two modes will result in a finite value of  $dcp$ , if the corona is not optically thick.

### 3 Analysis and Results

According to SOHO/LASCO CME catalog, the LE of whitelight CME in Figure 1 was at  $r_{cme} \approx 3.86R_\odot$  around  $\approx 06:48$  UT, nearly the same epoch as the GRAPH observations. But the centroids of the radio emission are located at  $r_{80} \approx 1.7 \pm 0.2R_\odot$  (80 MHz) and  $r_{53} \approx 2.1 \pm 0.2R_\odot$  (53 MHz). Therefore it is likely that the radio sources are not associated with the LE of the frontal structure in the whitelight CME. They seem to correlate spatially with parts of the frontal structure behind its LE. The separation between the centroids of the 80 MHz and 53 MHz radio sources in Figure 1 suggests possible density gradient in the frontal structure similar to that in the background corona since it is well known that radio emission from the Sun at a particular frequency ( $f$ ) can propagate towards the observer only from/above the critical level at which the plasma frequency ( $f_p$ ) corresponding to the local electron density ( $N_e$ ) equals  $f$ . Note that a gradually increasing  $N_e$  (towards the Sunward side) in the CME frontal structure is possible if there is material pile-up from lower coronal levels (P. Subramanian & Vourlidis, 2007; Bein et al., 2013). We generated a h-t plot using centroids of EUV eruptive activity, frontal structure of whitelight CME, and radio sources (Figure 4). To identify the centroids of EUV and whitelight structures, we fitted each of them with a circumcircle. The LE of the corresponding structure and the solar limb were assumed to be the upper and lower boundaries (e.g., Bein et al., 2013). The h-t measurements obtained with STEREO-A/COR1 were multiplied by  $1/\cos(24^\circ)$  to correct for projection effects. All the data points are reasonably well aligned with the linear least squares fit line. The speed

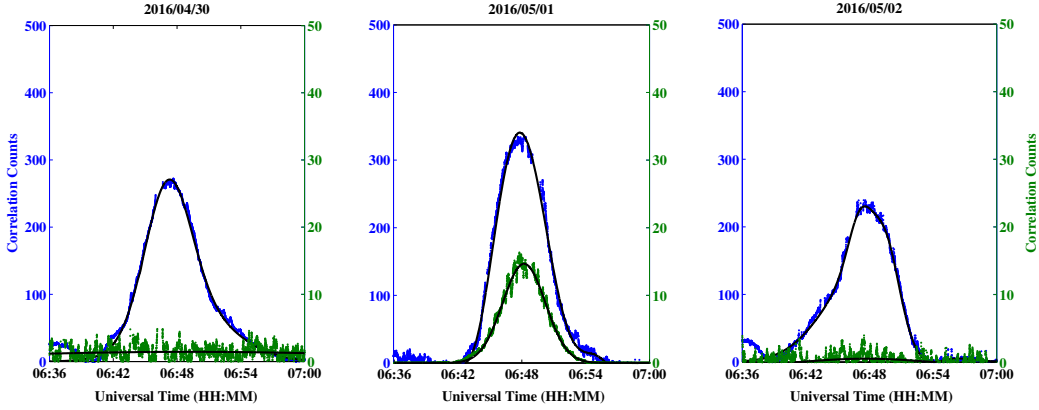


**Figure 3.** GRIP observations of Stokes I (‘blue’) and V (‘green’) emission at 80 MHz in the transit mode around 06:48 UT. The assymetry in the Stokes I observations on 2016 May 2 was due to a local radio frequency interference (RFI) around  $\approx 06:40$  UT. The ‘solid’ lines in black colour are the ‘fit’ to the respective data points.

of the CME ( $v_{cme}$ ) estimated from the aforesaid fit is  $\approx 233$  km/s. Note that since GRAPH observations were confined to 80 MHz and 53 MHz, there are only two data points from GRAPH.

It is known that the larger density gradient near the solar limb leads to refraction of low frequency radio waves. So, the contribution to observed thermal bremsstrahlung emission at any given frequency is primarily from regions well above the corresponding plasma level. This implies smaller optical depth ( $\tau$ ) since the absorption coefficient and hence  $\tau$  are maximum only near the plasma level (e.g., Smerd, 1950; Aubier et al., 1971; Vocks et al., 2018). In the case of solar corona,  $T_b$  and  $\tau$  are related to its electron temperature ( $T_e \approx 10^6$  K) as  $T_b \approx T_e(1 - e^{-\tau})$ . Since  $\tau$  above the limb is small as mentioned,  $T_b < T_e$  although the spectral index could be indicative of optically thick thermal emission. The emission from CMEs too undergo refraction and reflection near the plasma layer as described above (e.g., Bastian & Gary, 1997). The fact that  $T_b^{80}$  and  $T_b^{53}$  in the present case (see Section 2) are lesser than  $T_e$  also indicates the same. Note that since a CME contains primarily coronal material, its  $T_e$  is considered to be the same as that of the surrounding corona (e.g., Vourlidis, 2004). Using the aforementioned relation, we calculated  $\tau$  corresponding to  $T_b^{80}$  and  $T_b^{53}$ , and the values are  $\tau_{80} \approx 0.4$  and  $\tau_{53} \approx 0.1$ . These are reasonably consistent with  $\tau$  values for similar frequencies and at locations above the solar limb as in the present work (e.g., Smerd, 1950; Thejappa & Kundu, 1992; Vocks et al., 2018). Based on this, we then estimated  $N_e$  at  $r_{80} \approx 1.7 \pm 0.2 R_\odot$  and  $r_{53} \approx 2.1 \pm 0.2 R_\odot$  using the relation  $\tau = 2 \times 10^{-24} N_e^2 L T_e^{-1.5} f^{-2} \eta^{-1}$ , where  $L$  (cm) is the width of radio source along the line of sight and  $\eta = \sqrt{1 - 80.6 \times 10^6 N_e f^{-2}}$  is the refractive index (e.g., Sheridan & McLean, 1985). The lateral and radial widths of the radio sources in Figure 1 are  $w_{80} \approx 15' \times 16'$  (80 MHz) and  $w_{53} \approx 26' \times 29'$  (53 MHz). Assuming  $L$  as the average of lateral and radial widths, we find that  $N_e^{80} \approx 2.2 \times 10^7 \text{ cm}^{-3}$  at  $r_{80} \approx 1.7 \pm 0.2 R_\odot$  and  $N_e^{53} \approx 1.0 \times 10^6 \text{ cm}^{-3}$  at  $r_{53} \approx 2.1 \pm 0.2 R_\odot$ . These are in good agreement with our independent estimates of CME density using linearly polarized brightness (pB) measurements with STEREO-A/COR1 and the inversion technique based on spherically symmetric polynomial approximation (SSPA; solar.physics.montana.edu/wangtj/sspa.tar; Wang and Davila (2014); Wang et al. (2017)). At  $\approx 06:50$  UT (about the same time as GRAPH observations), we find  $N_e^{cor1a} \approx 4.8 \pm 1.4 \times 10^6 \text{ cm}^{-3}$  near  $r \approx 2.1 R_\odot$  (see Figure 2).

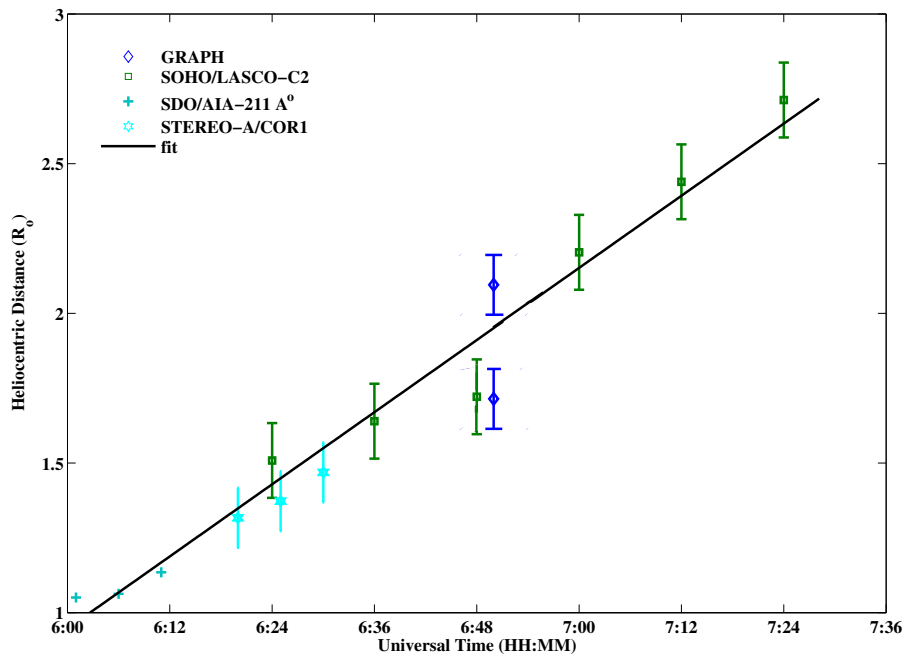


**Figure 4.** CME h-t plot obtained using EUV, whitelight and radio observations.



Considering the coronal plasma as fully ionized gas of normal solar composition (90% hydrogen and 10% helium by number), one finds that each electron is associated with approximately  $2 \times 10^{-24}$  g of material. Therefore the mass of the enhancement is given by  $M = 2 \times 10^{-24} N_e V$ , where  $V$  is the volume of enhancement. We calculated  $V$  as  $w_{80} \times L_{80}$  and  $w_{53} \times L_{53}$  at 80 MHz and 53 MHz, respectively. For  $N_e$  at the above two frequencies, we used  $N_e^{80}$  and  $N_e^{53}$  calculated earlier. Substituting for different values in the above relation, we get  $M_{80} \approx 1.3 \times 10^{16}$  g (80 MHz) and  $M_{53} \approx 3.4 \times 10^{15}$  g (53 MHz). The average of the above values is  $M_{cme}^{radio} \approx 7.4 \times 10^{15}$  g. Using this and  $v_{cme}$  mentioned earlier, we calculated the CME kinetic energy  $E_{cme}^{radio} \approx 2 \times 10^{30}$  erg. The estimates of  $M_{cme}^{radio}$  and  $E_{cme}^{radio}$  agree reasonably with the mass and kinetic energy of the CME estimated using SOHO/LASCO-C2 observations (see Section 2). Having said so, we would like to mention here that the values of  $M_{cme}^{radio}$  and  $E_{cme}^{radio}$  calculated above should be considered as upper limits due to lack of information on  $L$ . For example, if we assume that  $L$  is equal to density scale height in the corona (i.e.  $\approx 10^5$  km), then both  $M_{cme}^{radio}$  and  $E_{cme}^{radio}$  should be lesser by about an order of magnitude. So, the more appropriate results would be  $M_{cme}^{radio} \sim 10^{15}$  g and  $E_{cme}^{radio} \sim 10^{30}$  erg. Note that estimates of CME mass using whitelight coronagraph observations too are affected by uncertainties (Vourlidas et al., 2000; Carley et al., 2012; Bein et al., 2013).

Moving to magnetic field strength ( $B$ ) calculations, Sastry (2009) had shown earlier that if  $B \approx 0.5$  G and electron density is  $\approx 1.2 \times 10^6 \text{ cm}^{-3}$ , then it should be possible to observe circular polarized radio emission with  $dcp \approx 12\%$ . In the present case, the density at  $r \approx 2.1 R_\odot$  is  $\approx 1.0 \times 10^6 \text{ cm}^{-3}$  and the estimated  $dcp$  due to CME associated enhanced radio emission is  $\approx 12\%$  as mentioned earlier. Therefore it is likely that magnetic field strength in the CME at the above location is  $\approx 0.5$  G. This is close to some of the earlier reported  $B$  values at nearly the same heliocentric distance from other type of observations like non-thermal gyrosynchrotron emission from the CME loops (Bastian et al., 2001), geometrical properties of the CME flux rope and the shock at its leading edge (Gopalswamy et al., 2012), CME associated fast magnetosonic waves (Kwon et al., 2013), and second harmonic plasma emission from the CME leading edge (Hariharan et al., 2016a). Model calculations reported by Zucca et al. (2014) in connection with a CME associated coronal type II burst also predict nearly the same value of  $B$  at the above  $r$ .

## 4 Summary

We have presented evidence for enhanced thermal radio emission associated with the frontal structure of a CME (from just behind the limb of the Sun) that was observed with SOHO/LASCO-C2 on 2016 May 1. The radio data were obtained with GRAPH at 80 MHz and 53 MHz simultaneously. The plasma characteristics of the CME, estimated from radio observations, are:  $N_e \approx 2.2 \times 10^7 \text{ cm}^{-3}$  at  $r \approx 1.7 R_\odot$  and  $N_e \approx 1.0 \times 10^6 \text{ cm}^{-3}$  at  $r \approx 2.1 R_\odot$ ; mass and kinetic energy are  $\sim 10^{15}$  g and  $\sim 10^{30}$  erg, respectively; magnetic field strength is  $B \approx 0.5$  G at  $r \approx 2.1 R_\odot$ . Future observations with low frequency radio antenna arrays with larger collecting area like LOFAR and SKA should be able to effectively exploit this possibility for CMEs against the solar disk also (e.g., Ramesh, 2000c).

## Acknowledgments

We thank the staff of Gauribidanur observatory for their help in maintenance of antenna, receiver systems and the observations. Ajith Sampath and S. Kokila are thanked for their contributions to the work. The SOHO-LASCO CME catalog is generated and maintained at CDAW Data Center by NASA and Catholic University of America in cooperation with Naval Research Laboratory. The SDO/AIA data are courtesy of NASA/SDO and AIA science teams. The work of TJW was supported by NASA Cooperative Agreement NNG11PL10A to CUA and NASA grants 80NSSC18K1131 and 80NSSC18K0668. Data used in the study are at <https://www.iiap.res.in/gauribidanur/home.html>. We thank the referee for his/her comments which helped us to present the results in a better manner.

## References

- Aubier, M., Leblanc, Y., & Boischoat, A. (1971). Observations of the ‘quiet’ Sun at decameter wavelengths - Effects of scattering on the brightness distribution. *Astron. Astrophys.*, *12*, 435-441.
- Aurass, H. (1997). Coronal mass ejections and type II radio bursts. In G. Trotter (Ed.), *Coronal Physics from Radio and Space Observations: Lecture Notes in Physics* (Vol. 483, p. 135-160). doi: 10.1007/BFb0106455
- Bain, H. M., Krucker, S., Saint-Hilaire, P., & Raftery, C. L. (2014). Radio imaging of a type IVM radio burst on the 14th of August 2010. *Astrophys. J.*, *782*, 43. doi: 10.1088/0004-637X/782/1/43
- Bastian, T. S., & Gary, D. E. (1997). On the feasibility of imaging coronal mass ejections at radio wavelengths. *J. Geophys. Res.*, *102*, 14031-14040. doi: 10.1029/97JA00483
- Bastian, T. S., Pick, M., Kerdraon, A., Maia, D., & Vourlidas, A. (2001). The coronal mass ejection of 1998 April 20: Direct imaging at radio wavelengths. *Astrophys. J. Lett.*, *558*, L65-L69. doi: 10.1086/323421
- Bein, B. M., Temmer, M., Vourlidas, A., Veronig, A. M., & Utz, D. (2013). The height evolution of the ‘true’ coronal mass ejection mass derived from STEREO COR1 and COR2 observations. *Astrophys. J.*, *768*, 31. doi: 10.1088/0004-637X/768/1/31
- Benz, A. O., Monstein, C., Meyer, H., Manoharan, P. K., Ramesh, R., Altyntsev, A., ... Cho, K.-S. (2009). A world-wide net of solar radio spectrometers: e-CALLISTO. *Earth, Moon and Planets*, *104*, 277-285. doi: 10.1007/s11038-008-9267-6
- Brueckner, G. E., Howard, R. A., Koomen, M. J., Korendyke, C. M., Michels, D. J., Moses, J. D., ... Eyles, C. J. (1995). The Large Angle Spectroscopic Coronagraph. *Solar Phys.*, *162*, 357-402. doi: 10.1007/BF00733434
- Carley, E. P., McAteer, R. T. J., & Gallagher, P. T. (2012). Coronal mass ejection mass, energy, and force estimates using STEREO. *Astrophys. J.*, *752*, 36. doi: 10.1088/0004-637X/752/1/36
- Carley, E. P., Vilmer, N., Paulo, J. A. S., & Brian, O. F. (2017). Estimation of a coronal mass ejection magnetic field strength using radio observations of gyrosynchrotron radiation. *Astron. Astrophys.*, *608*, A137. doi: 10.1051/0004-6361/201731368
- Chrysaphi, N., Kontar, E. P., Holman, G. D., & Temmer, M. (2018). CME-driven shock and type II solar radio burst band splitting. *Astrophys. J.*, *868*, 79. doi: 10.3847/1538-4357/aae9e5
- Dulk, G. A. (1985). Radio emission from the Sun and stars. *Ann. Rev. Astron. Astrophys.*, *23*, 169-224. doi: 10.1146/annurev.aa.23.090185.001125
- Ebenezer, E., Ramesh, R., Subramanian, K. R., Sundara Rajan, M. S., & Sastri, C. V. (2001). A new digital spectrograph for observations of radio burst emission from the Sun. *Astron. Astrophys.*, *367*, 1112-1116. doi: 10.1051/0004-6361:20000540
- Ebenezer, E., Subramanian, K. R., Ramesh, R., Sundara Rajan, M. S., & Kathiravan, C. (2007). Gauribidanur radio array solar spectrograph. *Bull. Astron. Soc. India*, *35*, 111-119.
- Erickson, W. C., Gergely, T. E., Kundu, M. R., & Mahoney, M. J. (1977). Determination of the decameter wavelength spectrum of the ‘quiet’ Sun. *Solar Phys.*, *54*, 57-63. doi: 10.1007/BF00146425
- Gary, D. E. (2019). Cause and extent of the extreme radio flux density reached by the solar flare of 2006 December 06. In *Proc. 2008 ionospheric effects symposium*, eprint *arxiv:1901.09262*.
- Gary, D. E., Dulk, G. A., House, L. L., Illing, R., & Wagner, W. J. (1985). The type IV burst of 1980 June 29, 0233 UT - Harmonic plasma emission? *Astron. Astrophys.*, *152*, 42-50.

- Gopalswamy, N. (2006). Coronal mass ejections and type II radio bursts. In N. Gopalswamy, R. Mewaldt, & J. Torsti (Eds.), *Solar Eruptions and Energetic Particles: Geophys. Monograph Ser.* (Vol. 165, p. 207-220). doi: 10.1029/165GM20
- Gopalswamy, N., & Kundu, M. R. (1987). Simultaneous radio and white light observations of the 1984 June 27 coronal mass ejection event. *Solar Phys.*, *114*, 347-362. doi: 10.1007/BF00167350
- Gopalswamy, N., & Kundu, M. R. (1989). Radioheliograph and white-light coronagraph studies of a coronal mass ejection event. *Solar Phys.*, *122*, 145-173. doi: 10.1007/BF00162832
- Gopalswamy, N., & Kundu, M. R. (1990). Multiple moving magnetic structures in the solar corona. *Solar Phys.*, *128*, 377-397. doi: 10.1007/BF00838474
- Gopalswamy, N., & Kundu, M. R. (1992). Estimation of the mass of a coronal mass ejection from radio observations. *Astrophys. J. Lett.*, *390*, L37-L39. doi: 10.1086/186366
- Gopalswamy, N., & Kundu, M. R. (1993). Thermal and non-thermal emissions during a coronal mass ejection. *Solar Phys.*, *143*, 327-343. doi: 10.1007/BF00646491
- Gopalswamy, N., Nitta, N., Akiyama, S., Mäkelä, P., & Yashiro, S. (2012). Coronal magnetic field measurement from EUV images made by the Solar Dynamics Observatory. *Astrophys. J.*, *744*, 72. doi: 10.1088/0004-637X/744/1/72
- Hariharan, K., Ramesh, R., & Kathiravan, C. (2015). Observations of near-simultaneous split-band solar type II radio bursts at low frequencies. *Solar Phys.*, *290*, 2479-2489. doi: 10.1007/s11207-015-0761-5
- Hariharan, K., Ramesh, R., Kathiravan, C., Abhilash, H. N., & Rajalingam, M. (2016b). High dynamic range observations of solar coronal transients at low radio frequencies with a spectro-correlator. *Astrophys. J. Suppl.*, *222*, 21. doi: 10.3847/0067-0049/222/2/21
- Hariharan, K., Ramesh, R., Kathiravan, C., & Wang, T. J. (2016a). Simultaneous near-Sun observations of a moving type IV radio burst and the associated white-light coronal mass ejection. *Solar Phys.*, *291*, 1405-1416. doi: 10.1007/s11207-016-0918-x
- Howard, R. A., Moses, J. D., Vourlidas, A., Newmark, J. S., Socker, D. G., Plunkett, S. P., ... Carter, T. (2008). Sun-Earth Connection Coronal and Heliospheric Investigation. *Space Sci. Rev.*, *136*, 67-115. doi: 10.1007/s11214-008-9341-4
- Kathiravan, C., & Ramesh, R. (2004). Estimation of the three-dimensional space speed of a coronal mass ejection using metric radio data. *Astrophys. J.*, *610*, 532-536. doi: 10.1086/421381
- Kathiravan, C., & Ramesh, R. (2005). Identification of the source region of a 'halo' coronal mass ejection using meter wavelength radio data. *Astrophys. J. Lett.*, *627*, L77-L80. doi: 10.1086/431930
- Kathiravan, C., Ramesh, R., Indrajit V. Barve., & Rajalingam, M. (2011). Radio observations of the solar corona during an eclipse. *Astrophys. J.*, *730*, 91. doi: 10.1088/0004-637X/730/2/91
- Kathiravan, C., Ramesh, R., & Nataraj, H. S. (2007). The post-coronal mass ejection solar atmosphere and radio noise storm activity. *Astrophys. J. Lett.*, *656*, L37-L40. doi: 10.1086/512013
- Kathiravan, C., Ramesh, R., & Subramanian, K. R. (2002). Metric radio observations and ray-tracing analysis of the onset phase of a solar eruptive event. *Astrophys. J. Lett.*, *567*, L93-L95. doi: 10.1086/339801
- Kerdran, A., Pick, M., Trottet, G., Sawyer, C., Illing, R., Wagner, W. J., & House, L. L. (1983). The association of radio noise storm enhancements with the appearance of additional material in the corona. *Astrophys. J. Lett.*, *265*, L19-L21. doi: 10.1086/183950
- Kishore, P., Kathiravan, C., Ramesh, R., Rajalingam, M., & Indrajit V. Barve.

- (2014). Gauribidanur low frequency solar spectrograph. *Solar Phys.*, *289*, 3995-4005. doi: 10.1007/s11207-014-0539-1
- Kishore, P., Ramesh, R., Kathiravan, C., & Rajalingam, M. (2015). A low frequency radio spectropolarimeter for observations of the solar corona. *Solar Phys.*, *290*, 2409-2422. doi: 10.1007/s11207-015-0705-0
- Kumari, A., Ramesh, R., Kathiravan, C., & Gopalswamy, N. (2017a). New evidence for a coronal mass ejection driven high frequency type II burst near the Sun. *Astrophys. J.*, *843*, 10. doi: 10.3847/1538-4357/aa72e7
- Kumari, A., Ramesh, R., Kathiravan, C., & Wang, T. J. (2017b). Strength of the solar coronal magnetic field - a comparison of independent estimates using contemporaneous radio and white-light observations. *Solar Phys.*, *292*, 161. doi: 10.1007/s11207-017-1180-6
- Kumari, A., Ramesh, R., Kathiravan, C., Wang, T. J., & Gopalswamy, N. (2019). Direct estimates of the solar coronal magnetic field using contemporaneous extreme-ultraviolet, radio, and white-light observations. *Astrophys. J.*, *881*, 24. doi: 10.3847/1538-4357/ab2adf
- Kundu, M. R., Gergely, T. E., & Erickson, W. C. (1977). Observations of the ‘quiet’ Sun at meter and decameter wavelengths. *Solar Phys.*, *53*, 489-496. doi: 10.1007/BF00160291
- Kwon, R.-Y., Ofman, L., Olmedo, O., Kramar, M., Davila, J. M., Thompson, B. J., & Cho, K.-S. (2013). STEREO observations of fast magnetosonic waves in the extended solar corona associated with EIT/EUV waves. *Astrophys. J.*, *766*, 55. doi: 10.1088/0004-637X/766/1/55
- Lantos, P., Alissandrakis, C. E., Gergely, T. E., & Kundu, M. R. (1987). ‘Quiet’ Sun and slowly varying component at meter and decameter wavelengths. *Solar Phys.*, *112*, 325-340. doi: 10.1007/BF00148787
- Lemen, J. R., Title, A. M., Akin, D. J., Boerner, P. F., Chou, C., Drake, J. F., ... Edwards, C. G. (2012). The Atmospheric Imaging Assembly on the Solar Dynamics Observatory. *Solar Phys.*, *275*, 17-40. doi: 10.1007/s11207-011-9776-8
- Maguire, C. A., Carley, E. P., McCauley, J., & Gallagher, P. T. (2020). Evolution of the Alfvén Mach number associated with a coronal mass ejection shock. *Astron. Astrophys.*, *633*, A56. doi: 10.1051/0004-6361/201731368
- Maia, D. J. F., Gama, R., Mercier, C., Pick, M., Kerdraon, A., & Karlický, M. (2007). The radio coronal mass ejection event on 2001 April 15. *Astrophys. J.*, *660*, 874-881. doi: 10.1086/508011
- Mann, G., Classen, T., & Aurass, H. (1995). Characteristics of coronal shock waves and solar type II radio bursts. *Astron. Astrophys.*, *295*, 775-781.
- Mercier, C. (1996). Some characteristics of atmospheric gravity waves observed by radio interferometry. *Ann. Geophysicae*, *14*, 42-58. doi: 10.1007/s00585-996-0042-6
- Mondal, S., Oberoi, D., & Vourlidis, A. (2020). Estimation of the physical parameters of a CME at high coronal heights using low frequency radio observations. *Astrophys. J.*, *893*, 28. doi: 10.3847/1538-4357/ab7fab
- Monstein, C., Ramesh, R., & Kathiravan, C. (2007). Radio spectrum measurements at the Gauribidanur observatory. *Bull. Astron. Soc. India*, *35*, 473-480.
- Morosan, D. E., Kilpua, E. K. J., Carley, E. P., & Monstein, C. (2019). Variable emission mechanism of a type IV radio burst. *Astron. Astrophys.*, *623*, A63. doi: 10.1051/0004-6361/201834510
- Mugundhan, V., Hariharan, K., & Ramesh, R. (2017). Solar type IIIb radio bursts as tracers for electron density fluctuations in the corona. *Solar Phys.*, *292*, 155. doi: 10.1007/s11207-017-1181-5
- Mugundhan, V., Ramesh, R., Indrajit V. Barve., Kathiravan, C., Gireesh, G. V. S., Kharb, P., & Misra, A. (2016). Low frequency radio observations of the solar corona with arcminute angular resolution: Implications for coronal turbulence and weak energy releases. *Astrophys. J.*, *831*, 154. doi:

10.3847/0004-637X/831/2/154

- Mugundhan, V., Ramesh, R., Kathiravan, C., Gireesh, G., & Hegde, A. (2018b). Spectropolarimetric observations of solar noise storms at low-frequencies. *Solar Phys.*, *293*, 41. doi: 10.1007/s11207-018-1260-2
- Mugundhan, V., Ramesh, R., Kathiravan, C., Gireesh, G. V. S., Kumari, A., Hariharan, K., & Indrajit V. Barve. (2018a). The first low frequency radio observations of the solar corona on  $\approx 200$  km long interferometer baseline. *Astrophys. J. Lett.*, *855*, L8. doi: 10.3847/2041-8213/aaaf64
- Ramesh, R. (2000c). The ‘halo’ CME event Of 23 October 1997: Low frequency radio observations of the pre-event corona. *Solar Phys.*, *196*, 213-220. doi: 10.1023/A:1005288115027
- Ramesh, R. (2005a). Low frequency (30-110 MHz) radio imaging observations of solar coronal mass ejections. In K. P. Dere, J. Wang, & Y. Yan (Eds.), *Coronal and Stellar Mass Ejections: Proc. IAU Symp. 226* (p. 83-94). doi: 10.1017/S1743921305000190
- Ramesh, R. (2011a). Low frequency solar radio astronomy at the Indian Institute of Astrophysics. In A. R. Choudhuri & D. Banerjee (Eds.), *1st Asia-Pacific Sol. Phys. Meeting: Astron. Soc. India Conf. Ser.* (Vol. 2, p. 55-61).
- Ramesh, R. (2014). Solar observations at low frequencies with the Gauribidanur radioheliograph. In J. N. Chengalur & Y. Gupta (Eds.), *Metrewavelength Sky: Astron. Soc. India Conf. Ser.* (Vol. 13, p. 19-24).
- Ramesh, R., Anna Lakshmi, M., Kathiravan, C., Gopalswamy, N., & Umapathy, S. (2012a). The location of solar metric type II radio bursts with respect to the associated coronal mass ejections. *Astrophys. J.*, *752*, 107. doi: 10.1088/0004-637X/752/2/107
- Ramesh, R., Kathiravan, C., Indrajit V. Barve., & Rajalingam, M. (2012b). High angular resolution radio observations of a coronal mass ejection source region at low frequencies during a solar eclipse. *Astrophys. J.*, *744*, 165. doi: 10.1088/0004-637X/744/2/165
- Ramesh, R., Kathiravan, C., & Sastry, C. V. (2003). Metric radio observations of the evolution of a ‘halo’ coronal mass ejection close to the Sun. *Astrophys. J. Lett.*, *591*, L163-L166. doi: 10.1086/377162
- Ramesh, R., Kathiravan, C., & Sastry, C. V. (2010a). Estimation of magnetic field in the solar coronal streamers through low-frequency radio observations. *Astrophys. J.*, *711*, 1029-1032. doi: 10.1088/0004-637X/711/2/1029
- Ramesh, R., Kathiravan, C., & Satya Narayanan, A. (2011b). Low frequency observations of polarized emission from long-lived non-thermal radio sources in the solar corona. *Astrophys. J.*, *734*, 39. doi: 10.1088/0004-637X/734/1/39
- Ramesh, R., Kathiravan, C., Sreeja S. Kartha, & Gopalswamy, N. (2010b). Radioheliograph observations of metric type II bursts and the kinematics of coronal mass ejections. *Astrophys. J.*, *712*, 188. doi: 10.1088/0004-637X/712/1/188
- Ramesh, R., Kathiravan, C., Sundara Rajan, M. S., Indrajit V. Barve, & Sastry, C. V. (2008). A low frequency (30-110 MHz) antenna system for observations of polarized radio emission from the solar corona. *Solar Phys.*, *253*, 319-327. doi: 10.1007/s11207-008-9272-y
- Ramesh, R., Kishore, P., Sargam M. Mulay, Barve, I. V., Kathiravan, C., & Wang, T. J. (2013). Low frequency observations of drifting, non-thermal continuum radio emission associated with the solar coronal mass ejections. *Astrophys. J.*, *778*, 30. doi: 10.1088/0004-637X/778/1/30
- Ramesh, R., Kumari, A., Kathiravan, C., Ketaki, D., Rajesh, M., & Vrunda, M. (2020). Low frequency radio observations of the ‘quiet’ corona during the descending phase of sunspot cycle 24. *Geophys. Res. Lett.*, *47*, e2020GL090426. doi: 10.1029/2020GL090426
- Ramesh, R., Nataraj, H. S., Kathiravan, C., & Sastry, C. V. (2006a). The equatorial background solar corona during solar minimum. *Astrophys. J.*, *648*, 707-

711. doi: 10.1086/505677
- Ramesh, R., & Sastry, C. V. (2005b). Low frequency (<100 MHz) thermal radio emission from the solar corona and the effect of radial magnetic field. In K. Sankarasubramanian, M. Penn, & A. Pevtsov (Eds.), *Large-scale Structures and their Role in Solar Activity: ASP Conf. Ser.* (Vol. 346, p. 153-158).
- Ramesh, R., Subramanian, K. R., & Sastry, C. V. (1999a). Eclipse observations of compact sources in the outer solar corona. *Solar Phys.*, *185*, 77-85. doi: 10.1023/A:1005149830652
- Ramesh, R., Subramanian, K. R., & Sastry, C. V. (1999b). Phase calibration scheme for a “T” array. *Astron. Astrophys. Suppl.*, *139*, 179-181. doi: 10.1051/aas:1999387
- Ramesh, R., Subramanian, K. R., & Sastry, C. V. (2000b). Estimation of the altitude and electron density of a discrete source in the outer solar corona through low frequency radio observations. *Astrophys. Lett. & Comm.*, *40*, 93-102.
- Ramesh, R., Subramanian, K. R., Sundara Rajan, M. S., & Sastry, C. V. (1998). The Gauribidanur radioheliograph. *Solar Phys.*, *181*(2), 439-453. doi: 10.1023/A:1005075003370
- Ramesh, R., Sundara Rajan, M. S., & Sastry, C. V. (2006b). The 1024 channel digital correlator receiver of the Gauribidanur radioheliograph. *Exp. Astron.*, *21*, 31-40. doi: 10.1007/s10686-006-9065-y
- Ramesh, R., & Sundaram, G. A. S. (2000a). Type I radio bursts and the minimum between sunspot cycles 22 & 23. *Astron. Astrophys.*, *364*, 873.
- Sasikumar Raja, K., Ingale, M., Ramesh, R., Subramanian, P., Manoharan, P. K., & Janardhan, P. (2016). Amplitude of solar wind density turbulence from 10 to 45R<sub>⊙</sub>. *J. Geophys. Res.: Space Phys.*, *121*, 11605-11619. doi: 10.1002/2016JA023254
- Sasikumar Raja, K., Kathiravan, C., Ramesh, R., Rajalingam, M., & Indrajit V. Barve. (2013). Design and performance of a low frequency cross-polarized log-periodic dipole antenna. *Astrophys. J. Suppl.*, *207*(1), 2. doi: 10.1088/0067-0049/207/1/2
- Sasikumar Raja, K., & Ramesh, R. (2013). Low frequency observations of transient quasi-periodic radio emission from the solar atmosphere. *Astrophys. J.*, *775*, 38. doi: 10.1088/0004-637X/775/1/38
- Sasikumar Raja, K., Ramesh, R., Hariharan, K., Kathiravan, C., & Wang, T. J. (2014). An estimate of the magnetic field strength associated with a solar coronal mass ejection from low frequency radio observations. *Astrophys. J.*, *796*, 56. doi: 10.1088/0004-637X/796/1/56
- Sastry, C. V. (2009). Polarization of the thermal radio emission from outer solar corona. *Astrophys. J.*, *697*, 1934-1939. doi: 10.1088/0004-637X/697/2/1934
- Sheridan, K. V., Jackson, B. V., McLean, D. J., & Dulk, G. A. (1978). Radio observations of a massive, slow moving ejection of coronal material. *Publ. Astron. Soc. Aust.*, *3*, 249-250.
- Sheridan, K. V., & McLean, D. J. (1985). The ‘quiet’ sun at metre wavelengths. In D. J. McLean & N. R. Labrum (Eds.), *Solar Radiophysics: Study of Emission from the Sun at Metre Wavelengths* (p. 443-466).
- Smerd, S. F. (1950). Radio frequency radiation from the ‘quiet’ Sun. *Aust. J. Sci. Res. A*, *3*, 34-59. doi: 10.1071/PH500034
- Stewart, R. T., McCabe, M. K., Koomen, M. J., Hansen, R. T., & Dulk, G. A. (1974). Observations of coronal disturbances from 1 to 9R<sub>⊙</sub>. I: First event of 1973, January 11. *Solar Phys.*, *36*, 203-217. doi: 10.1007/BF00151561
- Stewart, R. T., & McLean, D. J. (1982). Correcting low frequency solar radio source positions for ionospheric refraction. *Publ. Astron. Soc. Aust.*, *4*, 386-389.
- Subramanian, K. R., & Sastry, C. V. (1988). The low frequency radio spectrum of the continuum emission from the ‘undisturbed’ Sun. *J. Astrophys. Astron.*, *9*, 225-229. doi: 10.1007/BF02715067

- Subramanian, P., & Vourlidas, A. (2007). Energetics of solar coronal mass ejections. *Astron. Astrophys.*, *467*, 685-693. doi: 10.1051/0004-6361/20066770
- Thejappa, G., & Kundu, M. R. (1992). Unusually low coronal radio emission at the solar minimum. *Solar Phys.*, *140*, 19-39. doi: 10.1086/528835
- Tun, S. D., & Vourlidas, A. (2013). Derivation of the magnetic field in a coronal mass ejection core via multi-frequency radio imaging. *Astrophys. J.*, *766*, 130. doi: 10.1088/0004-637X/766/2/130
- Vasanth, V., Chen, Y., Maoshui, L., Ning, H., Li, C., Feng, S., ... Du, G. (2019). Source imaging of a moving type IV solar radio burst and its role in tracking coronal mass ejection from the inner to the outer corona. *Astrophys. J.*, *870*, 30. doi: 10.3847/1538-4357/aeeffd
- Vocks, C., Mann, G., Breitling, F., Bisi, M. M., Dabrowski, B., Fallows, R., ... Rucker, H. (2018). LOFAR observations of the 'quiet' solar corona. *Astron. Astrophys.*, *614*, A54. doi: 10.1051/0004-6361/201630067
- Vourlidas, A. (2004). Radio observations of coronal mass ejections. In D. E. Gary & C. U. Keller (Eds.), *Solar and Space Weather Radio Physics: Astrophysics and Space Science Library* (Vol. 314, p. 223-242). doi: 10.1007/1-4020-2814-8\_11
- Vourlidas, A., Howard, R. A., Esfandiari, E., Patsourakos, S., Yashiro, S., & Michalek, G. (2010). Comprehensive analysis of coronal mass ejection mass and energy properties over a full solar cycle. *Astrophys. J.*, *722*, 1522-1538. doi: 10.1088/0004-637X/722/2/1522
- Vourlidas, A., Subramanian, P., Dere, K. P., & Howard, R. A. (2000). Large-Angle Spectrometric Coronagraph measurements of the energetics of coronal mass ejections. *Astrophys. J.*, *534*, 456-467. doi: 10.1086/308747
- Wagner, W. J., Hildner, E., House, L. L., Sawyer, C., Sheridan, K. V., & Dulk, G. A. (1981). Radio and visible light observations of matter ejected from the Sun. *Astrophys. J. Lett.*, *244*, L123-L126. doi: 10.1086/183495
- Wang, T., & Davila, J. M. (2014). Validation of spherically symmetric inversion by use of a tomographically reconstructed three-dimensional electron density of the solar corona. *Solar Phys.*, *289*, 3723-3745. doi: 10.1007/s11207-014-0556-0
- Wang, T., Reginald, N. L., Davila, J. M., St. Cyr, O. C., & Thompson, W. T. (2017). Variation in coronal activity from solar cycle 24 minimum to maximum using three-dimensional reconstructions of the coronal electron density from STEREO/COR1. *Solar Phys.*, *292*, 97. doi: 10.1007/s11207-017-1130-3
- Zucca, P., Pick, M., Demoulin, P., Kerdran, A., Lecacheux, A., & Gallagher, P. T. (2014). Understanding coronal mass ejections and associated shocks in the solar corona by merging multi-wavelength observations. *Astrophys. J.*, *795*, 68. doi: 10.1088/0004-637X/795/1/68